2018-01-0551 Published 03 Apr 2018

The Influence of Autonomous Driving on Passive Vehicle Dynamics

Tommaso Novi Universita degli Studi di Firenze

Alex Liniger ETH Zürich

Renzo Capitani Universita degli Studi di Firenze

Marco Fainello and Giacomo Danisi Danisi Engineering S.r.l.

Claudio Annicchiarico Meccanica 42 S.r.l.

Citation: Novi, T., Liniger, A., Capitani, R., Fainello, M. et al. "The Influence of Autonomous Driving on Passive Vehicle Dynamics," SAE Technical Paper 2018-01-0551, 2018, doi:10.4271/2018-01-0551.

Abstract

Traditional vehicles are designed to be inherently stable. This is typically obtained by imposing a large positive Static Margin (SM). The main drawbacks of this approach are the resulting understeering behaviour of the vehicle and, often, a decrease in peak lateral grip due to oversized rear tire characteristics. On the other hand, a lower SM can cause a greater time delay in the vehicle's response which hardens the control of a vehicle at limit handling for a human being. By introducing advanced autonomous driving features into future vehicles, the human factor can be excluded in limit handling manoeuvers (e.g. obstacle avoidance occurrences) and, consequently, the need for a high SM (i.e. high controllability for human drivers) can be avoided. Therefore, it could be possible to exploit the passive vehicle dynamics and enhance the performance, both in terms of peak grip and transient response.

The goal of this paper is to explore if a decrease in SM can lead to a performance advantage on an obstacle avoidance manoeuver when the vehicle is driven by a robotic controller. This is achieved by analyzing the behavior of various vehicle models with different SMs and peak lateral acceleration on a non-standard double lane change manoeuver. After having characterized the dynamic response of the various models in both steady-state and unsteady-state, several tests are run on a Driver-in-Motion (DiM) dynamic driving simulator driven by human drivers. The same tests are run again in a Model-in-the-Loop (MiL) simulation where the vehicle is controlled by means of a Nonlinear Model Predictive Control (NMPC). The results show that the robotic controller outperforms a human driver and poses interesting design challenges for autonomous vehicles.

Introduction

Commercial vehicles are typically designed to be stable. Consequently, these tend to have an understeering characteristic (under steady-state and linear tire range assumptions). These features are desired since they tend to make the vehicle safer and less prone to loss of control when external perturbations are applied. Additionally, understeering vehicles are more intuitive to drive since counter steering manoeuvers are generally not required. It is a well-known fact that understeering vehicles tend to saturate the front tires before the rear ones, thus decreasing the overall attainable peak lateral acceleration. Also, most of these vehicles tend to become unstable at higher accelerations ([1, 2, 3]). Over the last decades, many researchers have worked on active systems which allow to stabilize the vehicle [4]. Some of the first studies were by Bosch; their systems aim to stabilize a car in critical conditions driven by a human. The most important ones are the Vehicle Dynamics Control (VDC) System of Bosch [5] and the Electronic Stability Program (ESP) [6]. More recently many more types of control systems have been used to improve the vehicle stability considering also the influence of the driver as an external disturbance by means of robust control techniques [7]. Other types of vehicle stability controllers, which do not include the driver as an uncertainty, are based on adaptive sliding-mode [8], model predictive control (MPC) [9] and proportional-derivative control (PD) [10]. Additionally, researchers have worked on stability controllers considering uncertain [11] or unknown vehicle parameters which request prior identification [12]. Recently, stability has been studied for critical manoeuvers such as drifting ([13, 14]).

On the other hand, in the past few years, some research have studied how to optimize vehicle parameters to obtain the best performance from a vehicle considering a completely passive vehicle [15]. Also for active vehicles such as electric ones with four wheel torque vectoring, the passive vehicle dynamics has been analyzed to find the best configuration for time optimality [16]. These two works both use optimal control to compute the minimum time inputs. However, both of these consider offline optimization and simulation. To the authors' knowledge, until now nobody has studied how the passive vehicle dynamics can be modified with an autonomously controlled vehicle. With the recent development in autonomous vehicles, it could be possible to gain peak lateral grip despite the loss of open-loop stability. Some studies on pure vehicle stability for autonomous cars have been carried out recently [17].

By showing that an autonomous car can better handle the vehicle at its limits, the aim is to demonstrate that new horizons open up in the design of cars. Specifically, in this paper the effect of passive stability of a vehicle driven by a robotic controller rather than a human driver is analyzed. The goal is to show how passive stability can be drastically decreased for certain driving conditions. Thereby, the contributions can be summarized as follows, first, the limits of some reference drivers due to instability are determined. Therefore, several vehicle models were implemented in a numerical environment with different values of static margin and peak grip. These vehicles were then tested on several double lane change manoeuvers on a dynamic driving simulator. Second, we show that a nonlinear model predictive controller is able to go beyond the performance of the human drivers and successfully achieves the double lane change for all the tested models. Even though NMPC is an often proposed control technique for autonomous cars ([18, 19, 20]), in this paper we show that NMPC and unstable passive vehicle dynamics can be combined to achieve a more dynamically capable closed-loop system. Both a pure lateral controller and a combined lateral-longitudinal controller were implemented.

Note that we investigate a manoeuver where low passive stability is an advantage, however, for other situations high passive stability is still needed. Thus, additional active controls should be addressed to actively vary the passive stability depending on the driving situation, e.g. active roll stiffness.

The paper is organized as follows: first the different vehicle models are analyzed in terms of passive vehicle dynamics. Following, the manoeuver is described and the results obtained by different human drivers are shown. Finally, the NMPC controller and its results are shown.

Vehicle Stability

There are many ways to analyze the stability of a vehicle and different methods and metrics can be found in the literature [21]. Since the goal of this paper is to see the influence of the stability on autonomous vehicles, the well-known static margin (SM) is used to characterize the stability (under the assumptions of steady-state and linear tire range) [22]. Considering the following parameters, the wheelbase l, the front and rear wheelbase l_1 and l_2 respectively, the front and rear cornering stiffnesses C_1 and C_2 respectively, and the vehicle mass m, the SM can be defined as:

$$SM = \frac{1}{l} \cdot \left(\frac{l_2 C_2 - l_1 C_1}{C_1 + C_2} \right)$$

As for [23] the also well-known understeering gradient (UG) can be defined as:

$$UG = \frac{m}{l} \cdot \left(\frac{l_2 C_2 - l_1 C_1}{C_1 C_2} \right)$$

Hence:

- $UG = 0 \rightarrow SM = 0 \rightarrow Neutral\ vehicle$
- $UG > 0 \rightarrow SM > 0 \rightarrow Understeering\ vehicle$
- $UG < 0 \rightarrow SM < 0 \rightarrow Oversteering\ vehicle$

An understeering vehicle is stable for all conditions whilst an oversteering vehicle is unstable for velocities larger than the so called critical velocity [24].

To analyze the influence of the vehicle stability on the vehicle performance when driven autonomously, various configurations of the same vehicle with different static margins were implemented in the commercial software Vi-CarRealTime (Vi-CRT). The only variation made between the various models were the tires.

Tire Merging

The nominal vehicle considered is a RWD and front steering car with differentiated front and rear tires. The rear tires have higher grip compared to the front ones. The commercial software uses Pacejka Magic Formula (MF) [25] to model the tires. Specifically, MF 6.1 was used for this work. Starting from the original front and rear tires, six different tire models were created in the following way. Every i^{th} MF parameter p_i^k (for a total of N parameters) of the k^{th} tire model was obtained by interpolating linearly the correspondent i^{th} MF parameter of the original front p_i^f and rear p_i^r tires. For every k^{th} tire model, the merging factor of the interpolant line m^k (merge) was varied from 0 to 1 with a variation of 0.2 between model k and $(k-1)$ resulting in the following formulation:

$$p_i^k = (1 - m^k) \cdot p_i^r + m^k \cdot p_i^f \quad 0 \le m^k \le 1, m^k - m^{k-1} = 0.2$$
$$i = 1, \ldots, N$$

$$if\ m^k = 1 \quad \Rightarrow \quad p_i^k = p_i^f \quad \Rightarrow \quad Original\ front\ tire$$

$$if\ m^k = 0 \quad \Rightarrow \quad p_i^k = p_i^r \quad \Rightarrow \quad Original\ rear\ tire$$

The Pacejka parameters of the original model were found by fitting real data and were then used to validate the vehicle model with experimental results. The goal of the scaling process is to simulate tires with similar compound and construction but different size.

The results of the tire merging show that the pure longitudinal and lateral behavior (Figure 1) changes both in terms of peak friction coefficient μ_{peak} and cornering stiffness.

The latter is particularly true for the lateral behavior where also the decay after μ_{peak} is very low.

The combined force behavior (Figure 2) also shows that the lateral forces are more affected by the merging operation. The lateral $\mu_{y_{peak}}$ between the tire with highest grip and the

FIGURE 1 Tire merging results - pure longitudinal and lateral behavior.

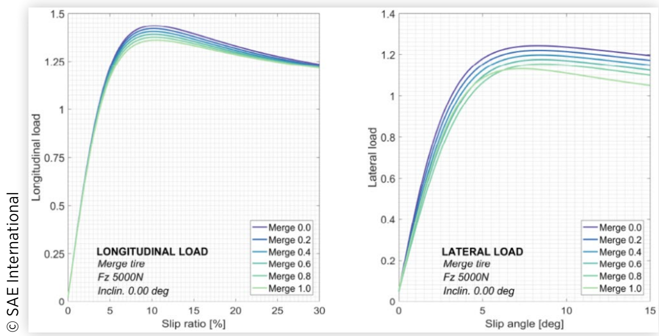

FIGURE 2 Tire merging results - combined force behavior.

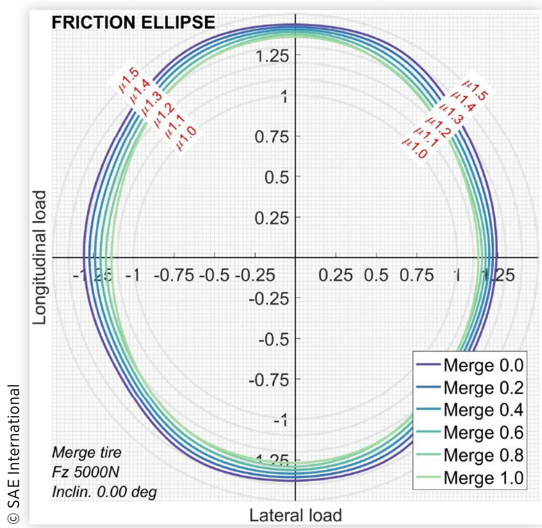

one with lowest is approximately 9% whilst the longitudinal one μ_{xpeak} is approximately only 5%.

Vehicle Configurations

With the six tire configurations, five different vehicle models were created. As previously mentioned, these vehicles have the same inertial properties, K&C characteristics and geometrical features. The goal was to obtain vehicles with different SM values and, consequently, peak performance. The various tire models used for the different models are shown in Table 1.

Where the vehicle at Step00 corresponds to the vehicle with the original tires. The open-loop behavior of these vehicles was analyzed in both steady-state and transient manoeuvers to obtain values of SM, peak lateral acceleration (for steady-state manoeuvers) and time delay.

TABLE 1 Vehicle configurations - tire models.

	Step 00	Step 02	Step 04	Step 06	Step 08
Front tire m^k	1	0.8	0.6	0.4	0.2
Rear tire m^k	0	0.2	0.4	0.6	0.8

Steady-State The steady-state behavior was analyzed by means of a ramp steer manoeuver and both the peak lateral acceleration and static margin were evaluated (Figure 3). The reference value of the latter for the various configurations was taken in the linear range of the tires, at a lateral acceleration of 0.2 g. The static margin varies from a value of +12% of the original vehicle to a value of −8% for Step08. Hence, the vehicle goes from being stable and understeering to being unstable and oversteering. This is the result of the merging tire process.

For Step00, the front tires saturate before the rear ones. The latter have a higher peak friction coefficient and, therefore, generate a large anti-yaw moment. The result is a vehicle with higher yaw damping, given also the higher rear cornering stiffness. The opposite is valid for Step08. The front to rear grip distribution is in favor of the front tires and the result is a vehicle with low yaw damping. However, the peak lateral acceleration also grows since both tires are close to the limit of adhesion contemporarily. Consequently, the lateral acceleration which the vehicle can sustain is higher. The values of static margin and peak lateral acceleration ($a_{y_{peak}}$) of the various models are shown in Table 2. The variation of these quantities for the different models with respect to the original vehicle have also been indicated.

Finally, since in the various vehicle configurations the lateral acceleration to steering angle relationship changes, due to the variation of the understeering gradient, the steering ratio of the different models was varied.

This was done so that the perceived behavior of the vehicle to a human driver would be the same for all vehicle models in steady-state. Specifically, the steering ratio was adapted to obtain the same lateral acceleration (0.5 g) for a given steering wheel angle (Figure 4).

Step Response The transient behavior was analyzed by means of a step steer manoeuver. This was done with the

FIGURE 3 Steady-state open-loop response - static margin and peak lateral acceleration.

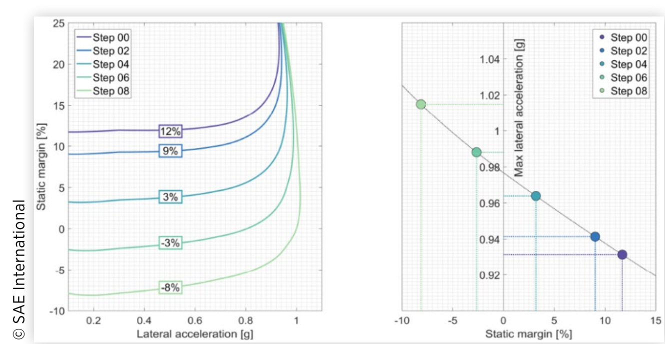

TABLE 2 Steady-state results.

	Step 00	Step 02	Step 04	Step 06	Step 08
$a_{y_{peak}}$ [g]	0.931	0.941	0.964	0.988	1.015
$\Delta a_{y_{peak}}$	-	+1.1%	+3.5%	+6.1%	+9.0%
SM @ 0.2g	12%	9%	3%	−3%	−8%
ΔSM @ 0.2g	-	−25%	−75%	−125%	−167%

FIGURE 4 Steady-state open-loop response - understeering gradient at 20 m/s. On the left the original steering ratio. On the right the corrected steering ratio.

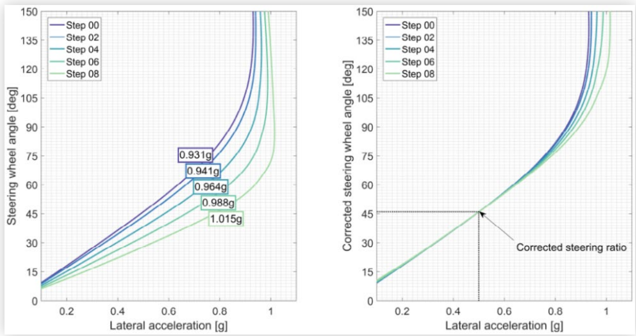

corrected steering ratio applied. With this manoeuver the time delay of both the lateral acceleration response and yaw rate response were evaluated (Figure 5). The metric to evaluate this was chosen as the time difference (Δt) between the peak value and 90% of that peak.

As the vehicle's SM decreases, the time delay increases. The reason is that the stable vehicle's larger front slip angles (lower cornering stiffness) are obtained mainly with larger toe angles, particularly in the first phase of the manoeuver.

Thus, since the toe angle variation has no delay, the rate of the front slip angles in the stable vehicle is greater than the one in the unstable vehicle. In the unstable vehicle, a larger contribution to the slip angle generation is given by lateral velocity and yaw rate. Since these are the time integral of yaw moment and lateral force which are caused by the slip angles themselves, these effects are slower than toe angle variation. The numeric values of this analysis are shown in Table 3. Since the manoeuver was performed with a forward velocity of

FIGURE 5 Step response - time delay of lateral acceleration and yaw rate variation with static margin.

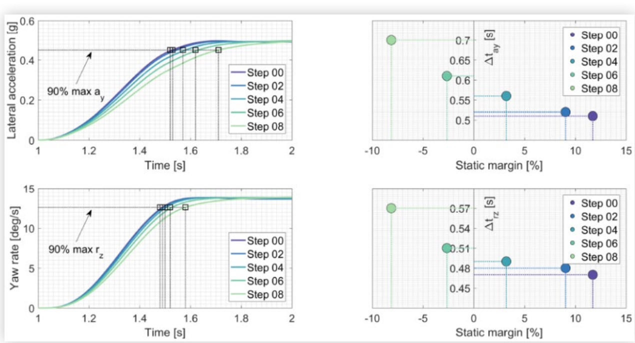

TABLE 3 Step response results.

	Step 00	Step 02	Step 04	Step 06	Step 08
Δt_{ay} [s]	0.51	0.52	0.56	0.61	0.70
Δs_{ay} [m]	10.2	10.4	11.2	12.2	14.0
Δlag_{ay}	-	+1.9%	+9.8%	+19.6%	+37.3%
Δt_r [s]	0.47	0.48	0.49	0.51	0.57
Δs_r [m]	9.4	9.6	9.8	10.2	11.4
Δlag_r	-	+2.1%	+4.2%	+8.5%	+21.3%

20 m/s, the delays in terms of space (Δs) have been calculated and so have lag variations (Δlag) with respect to the original configuration.

Test Manoeuver

A closed-loop avoidance manoeuver was defined which requests both large amounts of grip and stability in order to evaluate the role of a human driver in comparison to a robotic controller. The selected manoeuver (Figure 7) is a variation of the classic ISO double lane change manoeuver (ISO 3888). However, some of the parameters were varied in order to make it more similar to a real world avoidance manoeuver.

The manoeuver was first tested by human drivers on the Driver-in-Motion dynamic driving simulator installed at the Advanced Vehicle Dynamics center at Danisi Engineering. With the human tests it was possible to define one configuration of the manoeuver which exploited the limits of the reference human drivers on a highly unstable vehicle (configuration Step08). This same scenario was then used for the autonomous vehicle.

The lane offsets and widths were chosen similar to a typical lane found on country roads (approximately 3.75 m) and were kept constant throughout the study. The manoeuver execution was to arrive at 100 km/h (~28 m/s) through the first gate and lift off the throttle after passing the last cone of the entry gate. From then, the only input for the driver was the steering wheel until the end of the manoeuver. The velocity was guaranteed by adapting the gear ratios so that the driver could keep full throttle in second gear and maintain the rpm limiter and speed. The lift off adds additional instability due to the vertical load variation. To replicate an unplanned avoidance action, the steering wheel was kept to zero until passing the last cone, thus

FIGURE 6 DiM driver simulator.

FIGURE 7 Test manoeuver.

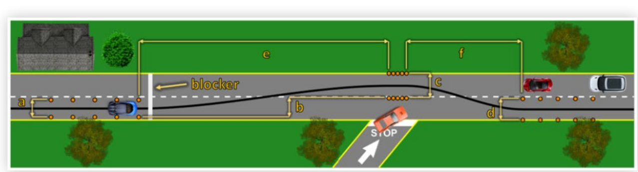

TABLE 4 Manoeuver geometry.

	a	b	c	d	e	f
Distance [m]	2.6	3.75	3.75	3.75	43	35-20
Variable	no	no	no	no	no	yes

eliminating the anticipation of the steering manoeuver. To guarantee no anticipation in the steering action, a graphical "blocker" of approximately 2 m of height which covers the entire width of the lane was added. Additionally, the direction of the obstacle (i.e. right or left) was completely random. The blocker made a big difference in the manoeuver success due to the impossibility to anticipate. In fact, with the introduction of the blocker a large delay was introduced (approximately 0.3-0.5 s and 8.4-14.0 m at 28 m/s). The entry width *a* was set to 2.6 m while the avoidance length *e* was set to 43 m. The latter was kept constant since the performance of the vehicle through the first lane change is largely a function of the reaction time of the driver, while the focus of this study is on the controllability rather than reaction times. The obstacle offset *b* was set to 3.75 m which is a typical lane width for a variety of roads including freeways, highways and main country roads. The idea of the setup is to model an avoidance manoeuver whereby the entire right lane is blocked by an obstacle. The avoidance lane width *c* was set to the same distance. This is different to the ISO standard which uses the vehicle width in the lane width calculations. However, this allows for a more road realistic situation. The second lane change represents a secondary avoidance manoeuver (e.g. from oncoming traffic). The recovery length *f* was found to have a large impact on the results of the manoeuver since it requests an inversion of the yaw rate vector direction which induces critical sideslip velocities, particularly in unstable vehicles. This distance was the only variable distance within the simulation and was swept from 35 m to 20 m with variations of 3 m between a test and another. Finally, the recovery lane width *d* was also set to 3.75 m and left constant. A summary of the geometrical features of the manoeuver is shown in Table 4.

Human Driver Results

Three different human drivers were used as a sample, all with significant simulator experience. The results shown represent the average result of the three drivers (Figure 8).

The tests for the human drivers were performed in the dynamic driving simulator using always the same motion cueing. The manoeuver success was defined as a passage of the entire obstacle without touching any cones. Every combination of vehicle static margin and recovery length was repeated ten times for each driver. This summed up to a total of three hundred data points. A correlation coefficient of approximately −0.7 was found between the recovery length and static margin (expressed as percentage points). Hence, every 1% decrease of static margin increases the required recovery distance by 0.7 m in the double lane change manoeuver for this particular test configuration with these reference drivers.

The vehicle with the highest peak grip (Step08) had very peculiar handling although it has more lateral grip capacity, its

FIGURE 8 Heat map of the human results - all configurations.

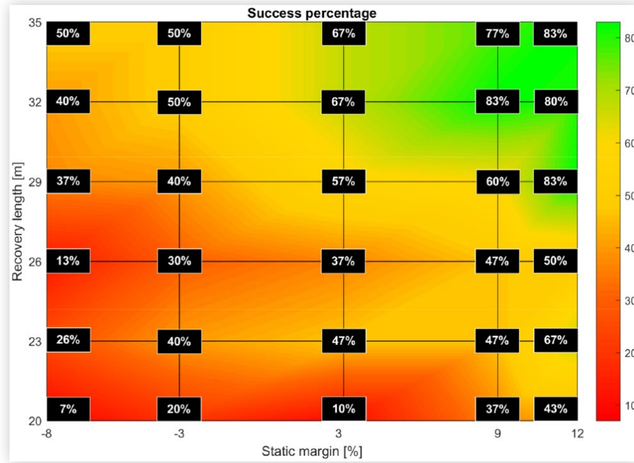

reaction to steering inputs is extremely slow (as expected from the results of the previous sections) to the point that any steering manoeuver required anticipation. The vehicle results in being practically unmanageable in transient changes of direction for a human driver due to the lack of rear cornering stiffness.

Autonomous Driver Results

An autonomous driver was developed to see the benefits of the "more unstable" vehicle. Unlike the human driver, a model predictive controller with a long enough prediction horizon and an accurate vehicle model allows to keep the lag effects into account. For this reason a NMPC was developed based on a validated seven degrees of freedom model (DOF). The controller sends the inputs and gets the feedback from the same Vi-CRT vehicle model used in the DiM. Another advantage of an MPC is that it is possible to use constraints, this allows to use the road boundaries as constraints and also limit the inputs. Two types of controllers were developed, a pure lateral one, where only the steering is actuated and a combined lateral-longitudinal controller, where also the throttle and brake pedals can be actuated. The former controller is the one used to compare the benefits of different vehicle configurations when driven autonomously. The latter controller was used only to evaluate the benefits of combined slip and inputs but does not represent a comparison with the human driver. In the MPC setup this is a straight forward extension of the lateral controller.

Controller Overview

The controller developed is a NMPC based on a previously developed framework ([26, 27]). The vehicle model considered is a rigid body (pitch, roll, heave and warp are neglected) describing the global position in the $X - Y$ plane, its global orientation Ψ and the center of gravity (COG) velocities v_x, v_y

and r_z in an orthonormal reference frame with origin in the COG. The z-axis points upwards. The remaining DOFs are the four wheel velocities w_{ij}, with i being front (1) or rear (2) axis and j being left (1) or right (2) side. Finally, the load transfers are modeled as first order systems. The dynamic longitudinal ΔF_{zX} and lateral ΔF_{zY} load transfers are then used to calculate the vertical loads. A static load transfer cannot be used, since an algebraic loop is present. The loop in the equality constraints is eliminated with a dynamic formulation. The slip ratios and slip angles are calculated with a kinematic formulation. The tire forces are evaluated with a full MF formulation whilst the aligning torques M_{zij} are neglected due to required computation time. The aero forces are also neglected (see previous work for full set of equations [26]).The reference line C, is transformed by describing it with a curvilinear abscissa approach. Thus, it can be expressed as a function of its curvature k and the parametrization of the curve by its arc-length s. With this approach, the states X, Y and Ψ can be replaced by the longitudinal position on the reference line s, the lateral error with respect to it $n = \|(X, Y)T - (XC, YC)T\|_2$ and the heading angle error with respect to it $\alpha = \Psi - \theta$. The road heading angle θ and (XC, YC) may be calculating by integrating the curvature as follows:

$$\frac{d\theta}{ds} = k(s); \quad \frac{dX^C}{ds} = \cos(\theta); \quad \frac{dY^C}{ds} = \sin(\theta)$$

The new states can be found with the following set of equations:

$$\dot{s} = \frac{v_x cos\alpha - v_y sin\alpha}{1 - nk(s)}$$

$$\dot{n} = v_x sin\alpha + v_y cos\alpha$$

$$\dot{\alpha} = \Omega - \frac{v_x cos\alpha - v_y sin\alpha}{1 - nk(s)} k(s)$$

The reference path of the NMPC is the centerline between the cones interpolated with a piecewise cubic Hermite interpolating polynomial [28]. However, only after that the vehicle has passed the blocker the obstacles (constraints) are available and the path is generated. This way the robotic controller gets the obstacle information at the same position as the human. Once the vehicle passed the blocker and the reference path is available, the error input signal to the controller is different to zero and the online optimization of the NMPC begins.

FIGURE 9 Road tracking.

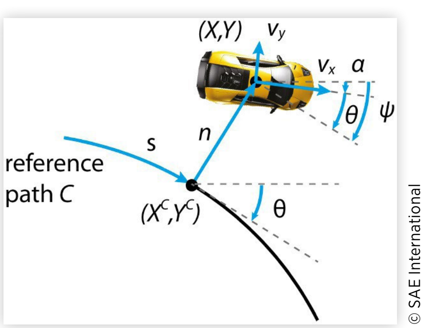

Until this point an open-loop full throttle and no steering policy is used just like for the human.

At this point, being x the state vector and u the input vector, the state space form set of equations becomes the following:

$$x(t) = \{s, n, \alpha, v_x, v_y, r_z, \omega_{ij}, \Delta F_{zX}, \Delta F_{zY}\}$$

$$\dot{x}(t) = f(t, x(t), u(t))$$

Where the system of equation is valid under the assumption that the vehicle never stops (only necessary when transforming all states), i.e. $v_x > 0$, and the vehicle always stays at a lateral distance n that is greater than the distance of the local center of curvature of the road, i.e. $n < k(s)$. A model transformation from time-dependent vehicle dynamics to track-dependent (spatial) dynamics is then proposed. This allows a natural formulation of obstacles and general road bounds under varying vehicle speed. The independent variable of the problem becomes s and no longer time t. This allows to eliminate one equation in the state space, reducing it to 11.

The final state space is the following:

$$\dot{x} = \frac{dx}{dt} = \frac{dx}{ds}\frac{ds}{dt} = \dot{s}x' \Rightarrow x'(s) = \frac{f(x(t), u(t))}{\dot{s}} = \tilde{f}(s, x(s), u(s))$$

$$x(s) = \{n, \alpha, v_x, v_y, r_z, \omega_{ij}, \Delta F_{zX}, \Delta F_{zY}\}$$

The set of equations is not singular only and if $\dot{s} > 0$.

The optimization problem is the following:

$$\min_{x(s),\, u(s)} \int_{s_0}^{s_f} \left(\| x(\sigma) - x_{ref}(\sigma) \|_Q^2 + \| u(\sigma) \|_R^2 + \| \dot{u}(\sigma) \|_S^2 \right) d\sigma$$

$$\begin{aligned} s.t. \quad & x'(s) = \tilde{f}(s, x(s), u(s)) \\ & n(s) \in [n_{\inf}(s), n_{\sup}(s)] \\ & u(s) \in [u_{\inf}(s), u_{\sup}(s)] \\ & \dot{u}(s) \in [\dot{u}_{\inf}(s), \dot{u}_{\sup}(s)] \\ & x(s_0) = x_0 \end{aligned}$$

For the implementation of the NMPC, Forces Pro [29] is used, and the included implicit Runge-Kutta method is used to discretize the above formulated NMPC problem. For the controller, only the most critical configurations were tested, thus, the manoeuver with recovery length equal to 20 m and the vehicle model Step08. However, to be able to compare the results with the human ones, also the original vehicle, configuration Step00 was tested. One of the 7% of the success manoeuvers of the human drivers for Step08 was selected as a reference. Unlike the human driver, the results of the NMPC controller is repeatable under ideal conditions. Note that, to be able to compare the passive vehicle dynamics for autonomous driving and not the performance of the controller itself, the controller was tuned for configuration Step08. The same tuning was then used for Step00. However, it could be possible to improve the performance of the original vehicle by properly tuning the controller.

The results shown in this section have been obtained without considering any external disturbances or parameter uncertainty, a separate study would be necessary to investigate the controller's performance in presence of such uncertainties. However, the goal of this paper is analyze how the passive stability can be varied comparing a robotic controller with a human driver and not to design the perfect autonomous driver. Therefore, the only model uncertainty is the simplifications in tire and vehicle models.

Lateral Controller Results

The lateral controller has the steering angle δ as the only input command, the driving torque C_m and braking torque C_b are kept constant and equal to zero. The steering wheel angle velocity is constrained to a value of 1000 deg/s. Note that the longitudinal equations are maintained in the controller's equality constraints since for this manoeuver, particularly with the unstable vehicle, it is expected to drive at high sideslip angles, thus combined slip effects and induced drag become relevant. This controller was used to compare the human driver to the robotic controller. The goal of the paper is to show that with autonomous vehicles, it is possible to rethink how commercial vehicles are designed from a passive vehicle dynamics perspective. It is possible to increase the instability gaining performance in terms of peak grip despite the increase of time delay. The latter is very well dealt by the NMPC as will be shown now.

The steering profiles and positions in the $X - Y$ plane (Figure 10) show that as expected, the reaction time of the controller is much faster than the human driver. In fact, the blocker does not influence the delay in the response, unlike for the human. This simplifies a lot the manoeuvre for the controller as it is not required to increase the steering angle and incur into high sideslip angles, especially for the unstable vehicle. While for the human driver the steering profile for the stable vehicle is much smoother than the unstable one, for the NMPC the unstable vehicle has a much smoother profile. This is due to the fact that the controller is predictive, hence the future time delays are modeled. Thus, since the unstable model has very little yaw damping due to the low rear cornering stiffness, its turning capacity is very high, this allows to actually anticipate the manoeuver and steer less. On the other hand, the stable vehicle is harder to drive for the controller since the controllable front wheels are near the saturation and have lower grip, additionally to the high yaw damping given by the rear axle. As a result, the unstable configurations has a higher safety margin from the constraints compared to the stable one. Also note that the controller tuning was obtained using the unstable vehicle, thus proper tuning could improve the performance.

The peaks and pits of the steering profiles of the controller are more numerous compared to the human driver. This is the big advantage of having a motor with high power controlling the steering wheel instead of a human. However, this also results in a very unnatural way of driving. Each steering manoeuver has in fact a counter steering input to stabilize the vehicle. One of the key aspects is that the human driver necessitates high lateral acceleration (Figure 11) due to the delays. Contrarily, the lateral accelerations of the controller are far from the vehicle's full potential because of the prediction horizon. Also, although the yaw rate for the robotic controller oscillates a lot resulting in a jerkier manoeuver, the maximum and average values are much lower. As expected, even with a smoother steering angle profile, the unstable configuration for the controller reaches higher yaw rates and sideslip angles in the second avoidance manoeuver where the yaw rate vector sign inversion and high sideslip velocities are requested.

The human driver and robotic controller for the two configurations are compared (Figure 12) using different metrics and plotting them in a spider plot. In particular, it is interesting to notice the different steering requests for the

FIGURE 10 Lateral controller results - position and steering profiles.

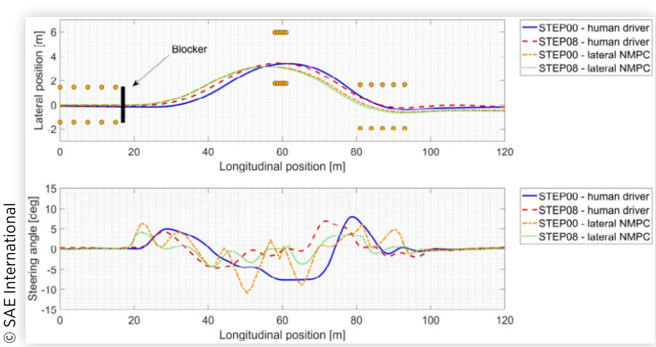

FIGURE 11 Lateral controller results - lateral acceleration, yaw rate and sideslip angle profiles.

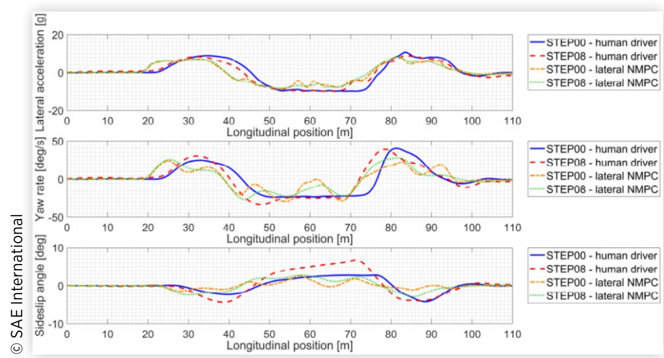

FIGURE 12 Lateral controller results - spider plot.

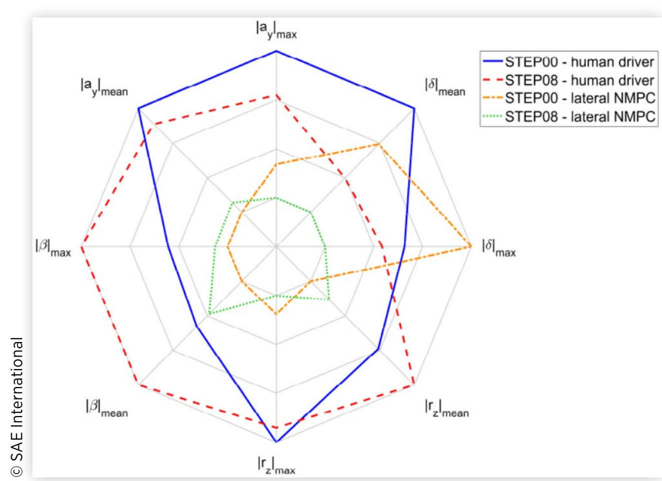

various cases ($|\delta|_{mean}$, $|\delta|_{max}$), how much lateral acceleration is needed to complete the manoeuver and how much grip is consequently still available ($|a_y|_{mean}$, $|a_y|_{max}$) and finally, how much the vehicle is actually turning and slipping with the given steering profile ($|r_z|_{mean}$, $|r_z|_{max}$, $|\beta|_{mean}$, $|\beta|_{max}$). The results show that the unstable vehicle controlled by the NMPC has better values respect to both to the stable vehicle driven by the robotic controller and the human driver in both configuration.

Combined Controller Results

Since the maximum lateral acceleration of the lateral controller was far from the peak, in this section we test if the additional control authority of a combined controller can further improve the performance. The execution of the manoeuver is still the same, with the lift off at the last cone and start of the inputs only after the blocker. However, this time the controller can also brake or accelerate. To make sure the vehicle would complete the manoeuver in the quickest time possible (to exploit the vehicles performance), an additional cost $|| \Delta V ||_T^2$ was added to the NMPC cost function. This cost is on the difference in the vehicle's forward velocity and the initial manoeuver speed. Once again, the tuning of the controller was done on the configuration Step08.

During the first steering manoeuver (Figure 13), the combined controller reaches higher steering angles, lateral accelerations, sideslip angles and yaw rates. This is due to the controller braking as it enters the other lane. This induces an even larger weight transfer, reducing the yaw damping. However, because the front tires are working under combined slip and the cornering stiffness is lower, the steering angle requested is higher. The steering angle profiles of the combined controllers are smoother than the pure lateral ones due to the combined effects (which gives induced yaw moments) and the possibility of varying the speed with the longitudinal controls.

During the second avoidance, the sideslip angle and yaw rate of the combined controller on the unstable vehicle reaches much higher values than the lateral controller. This is because after the first braking manoeuver, the controller forces the vehicle to accelerate reducing the lateral force produced by the rear tires. The combined controller spider plot (Figure 15) looks very similar to that of the human driver (Figure 12) but with a similar steering profile to the lateral controller.

FIGURE 13 Combined controller results - position and steering profiles.

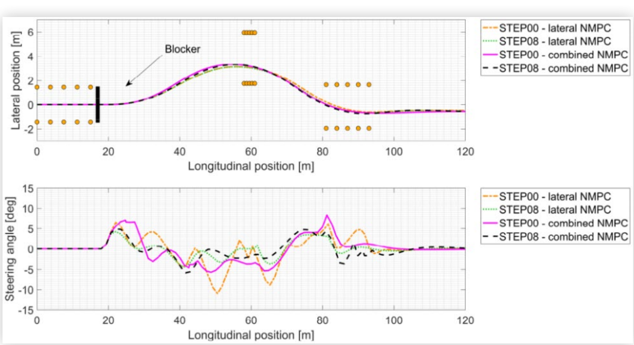

FIGURE 14 Combined controller results - lateral acceleration, yaw rate and sideslip angle profiles.

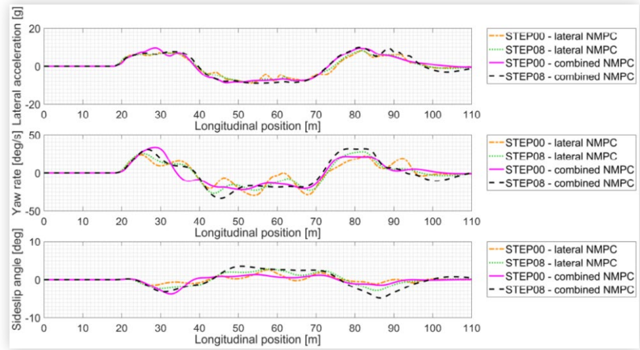

FIGURE 15 Combined controller results - spider plot comparing.

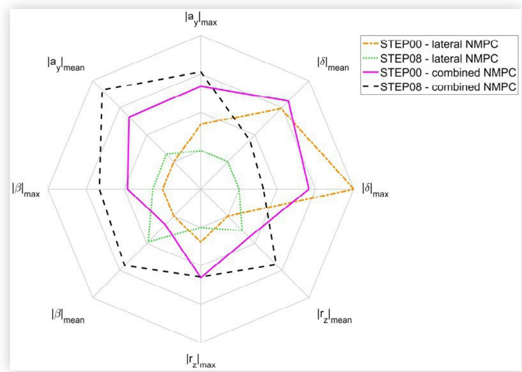

However, even if the accelerations are very similar, the sideslip angle and yaw rate are much lower, showing that even with an unstable vehicle, the robotic controller is capable of maintaining high controllability. The combined controller spider plots are larger than the lateral controller ones since the manoeuver execution time for the former is significantly lower than the latter and more grip is used. Furthermore, the combined controller on the unstable vehicle has a lower execution time and higher accelerations than the stable vehicle controller by the NMPC.

Conclusions

A sweep of manoeuver geometry and vehicle stability showed the dependence of both parameters on the ability to perform a closed-loop avoidance manoeuver. Both a series of human drivers and NMPC controllers were compared through the same sweep of vehicle stability and manoeuver geometry. The robotic controller completed all of the setups and manoeuver geometries successfully but the unstable setups required piloting in a very unnatural way in order to keep the vehicle response damped. The possibility of controlling both the longitudinal and the lateral behavior showed great advantages. The results obtained open up new possibilities in the design of passive vehicle dynamics with autonomous vehicles. Particularly, the passive stability could be varied depending on the driving situation in order to exploit the vehicle performance. A vehicle with lower static margin gains in peak lateral performance and in this paper it has been shown that, unlike a human driver, a robotic controller can take advantage of this despite the lower stability. In future work it would be interesting to investigate low level controls which allow changing the static margin to adjust to a given task to get the best of both worlds.

References

1. Bundorf, R.T., "The Influence of Vehicle Design Parameters on Characteristic Speed and Understeer," SAE Technical Paper 670078, 1967 10.4271/670078.
2. Allen, R.W., Myers, T.T., Rosenthal, T.J., and Klyde, D.H., "The Effect of Tire Characteristics on Vehicle Handling and Stability," SAE Technical Paper 2000-01-0698, 2000, doi:10.4271/2000-01-0698.
3. Hac, A. and Bodie, M.O., "Improvements in Vehicle Handling through Integrated Control of Chassis Systems," *International Journal of Vehicle Autonomous Systems* 1(1):83, 2002, doi:10.1504/IJVAS.2002.001807.
4. Mousavinejad, I.E., Zhu, Y., and Vlacic, L., "Control Strategies for Improving Ground Vehicle Stability: State-Of-The-Art Review," Control Conference (ASCC), 2015 10th Asian, IEEE: 1-8, 2015.
5. Zanten, A.T. van, Erhardt, R., and Pfaff, G., "VDC, The Vehicle Dynamics Control System of Bosch," SAE Technical Paper 950759 1995, doi:10.4271/950759.
6. Van Zanten, A.T., "Bosch ESP Systems: 5 Years of Experience," SAE Technical Paper 2000-01-1633, 2000, doi:10.4271/2000-01-1633.
7. Carvalho, A., Palmieri, G., Tseng, H.E., Glielmo, L., et al., "Robust Vehicle Stability Control with an Uncertain Driver Model," Control Conference (ECC), 2013 European, IEEE: 440-445, 2013.
8. Le, A.-T. and Chen, C.-K., "Vehicle Stability Control by Using an Adaptive Sliding-Mode Algorithm," *International Journal of Vehicle Design* 72(2):107-131, 2016.
9. Jalali, M., Hashemi, E., Khajepour, A., Chen, S., and Litkouhi, B., "A Combined-Slip Predictive Control of Vehicle Stability with Experimental Verification," *Vehicle System Dynamics* 56:319-340, 2017, doi:10.1080/00423114.2017.1376751.
10. Lu, J., Xu, L., Eisele, D., Samuel, S. et al., "An Advanced Yaw Stability Control System," SAE Technical Paper 2017-01-1556, 2017, doi:10.4271/2017-01-1556.
11. Huijun, G., Weichao, S., Shen, Y., and Kaynak, O., "Stability Control for Lateral Vehicle Motion with Uncertain Parameters and External Nonlinearities," Control Conference (CCC), 2013 32nd Chinese: 2733-2738, 2013.
12. Shraim, H., Ouladsine, M., Fridman, L., and Romero, M., "Vehicle Parameter Estimation and Stability Enhancement Using Sliding Modes Techniques," *International Journal of Vehicle Design* 48(3-4):230-254, 2008.
13. Velenis, E., Katzourakis, D., Frazzoli, E., Tsiotras, P., et al., "Stabilization of Steady-State Drifting for a RWD Vehicle," Proceedings of AVEC, 2010.
14. Edelmann, J. and Plöchl, M., "Handling Characteristics and Stability of the Steady-State Powerslide Motion of an Automobile," *Regular and Chaotic Dynamics* 14(6):682-692, 2009, doi:10.1134/S1560354709060069.
15. Perantoni, G. and Limebeer, D.J.N., "Optimal Control for a Formula One Car with Variable Parameters," *Vehicle System Dynamics* 52(5):653-678, 2014, doi:10.1080/00423114.2014.889315.
16. Smith, E.N., Velenis, E., Tavernini, D., and Cao, D., "Effect of Handling Characteristics on Minimum Time Cornering with Torque Vectoring," *Vehicle System Dynamics* 56:221-248, 2017, doi:10.1080/00423114.2017.1371771.
17. Mastinu, G., Della Rossa, F., Gobbi, M., and Previati, G., "Bifurcation Analysis of a Car Model Running on an Even Surface - a Fundamental Study for Addressing Automomous Vehicle Dynamics," *SAE Int. J. Veh. Dyn. Stab. NVH* 1(2), 2017, doi:10.4271/2017-01-1589.
18. Gao, Y., Gray, A., Frasch, J.V., Lin, T., et al., "Spatial Predictive Control for Agile Semi-autonomous Ground Vehicles," Proceedings of the 11th International Symposium on Advanced Vehicle Control, 2012.
19. Verschueren, R., De Bruyne, S., Zanon, M., Frasch, J.V., et al., "Towards Time-Optimal Race Car Driving Using Nonlinear MPC in Real-Time," Decision and Control (CDC), 2014 IEEE 53rd Annual Conference on, IEEE: 2505-2510, 2014.
20. Liniger, A., Domahidi, A., and Morari, M., "Optimization-Based Autonomous Racing of 1:43 Scale RC Cars," *Optimal Control Applications and Methods* 36(5):628-647, 2015, doi:10.1002/oca.2123.
21. Liu, W., Xiong, L., Leng, B., Meng, H. et al., "Vehicle Stability Criterion Research Based on Phase Plane Method," SAE Technical Paper 2017-01-1560, 2017, doi:10.4271/2017-01-1560.
22. Milliken, W.F. and Milliken, D.L., "*Race Car Vehicle Dynamics*," (Warrendale, SAE International, 1995), ISBN 978-1-56091-526-3.
23. Guiggiani, M., "*Dinamica del veicolo*," (Torino, CittàStudi, 2007), ISBN 978-88-251-7300-0.
24. Genta, G., "*Meccanica dell'autoveicolo*," (Torino, Levrotto & Bella, 2000), ISBN 978-88-8218-042-3.
25. Pacejka, H.B., "*Tire and Vehicle Dynamics*," (Warrendale, Society of Automotive Engineers), 2002, ISBN 978-0-7680-1126-5.
26. Frasch, J.V., Gray, A., Zanon, M., Ferreau, H.J., et al., "An Auto-Generated Nonlinear MPC Algorithm for Real-Time Obstacle Avoidance of Ground Vehicles," Control Conference (ECC), 2013 European, IEEE: 4136-4141, 2013.
27. Zanon, M., Frasch, J.V., and Diehl, M., "Nonlinear Moving Horizon Estimation for Combined State and Friction Coefficient Estimation in Autonomous Driving," Control Conference (ECC), 2013 European, IEEE: 4130-4135, 2013.
28. Fritsch, F.N. and Carlson, R.E., "Monotone Piecewise Cubic Interpolation," *SIAM Journal on Numerical Analysis* 17(2):238-246, 1980.
29. Zanelli, A., Domahidi, A., Jerez, J., and Morari, M., "FORCES NLP: An Efficient Implementation of Interior-Point Methods for Multistage Nonlinear Nonconvex Programs," *International Journal of Control*1-17, 2017, doi:10.1080/00207179.2017.1316017.

Contact Information

Corresponding author
Tommaso Novi
Department of Industrial Engineering (DIEF)
Università degli Studi di Firenze
Via di Santa Marta 3-50139 Firenze - Italia
Phone: (+39) 055 275 8707
tommaso.novi@unifi.it

Acknowledgments

The author would like to thank Meccanica 42 S.r.l., Danisi Engineering S.r.l. and Embotech GmbH for supporting this research.

Abbreviations

COG - Center Of Gravity

DiM - Driver-In-Motion

DOF - Degrees Of Freedom

ESP - Electronic Stability Program

ISO - International Standards Organization

K&C - Kinematics and Compliance

MF - Magic Formula

MiL - Model in the Loop

MPC - Model Predictive Control

NMPC - Nonlinear Model Predictive Control

PD - Proportional-Derivative

RWD - Rear Wheel Drive

SM - Static Margin

UG - Understeering Gradient

VDC - Vehicle Dynamic Control

Vi-CRT - Vi-CarRealTime

ISSN 0148-7191